Journal of Cosmology and Astroparticle Physics
An IOP and SISSA journal

Two types of softening detected in x-ray afterglows of Swift bursts: internal and external shock origins?

Y-P Qin[1,2], A C Gupta[3,1], J H Fan[1] and R-J Lu[2]

[1] Center for Astrophysics, Guangzhou University, Guangzhou 510006, People's Republic of China
[2] Physics Department, Guangxi University, Nanning 530004, People's Republic of China
[3] Aryabhatta Research Institute of Observational Sciences (ARIES), Manora Peak, Nainital-263129, India
E-mail: ypqin@gzhu.edu.cn, acgupta30@gmail.com, jhfan_cn@yahoo.com.cn and luruijing@126.com

Received 13 August 2008
Accepted 23 October 2008
Published 10 November 2008

Online at stacks.iop.org/JCAP/2008/i=11/a=004
doi:10.1088/1475-7516/2008/11/004

Abstract. The softening process observed in the steep decay phase of early x-ray afterglows of Swift bursts has remained a puzzle since its discovery. The softening process can also be observed in the later phase of the bursts and its cause has also been unknown. Recently, it was suggested that, influenced by the curvature effect, emission from high latitudes would shift the Band function spectrum from a higher energy band to a lower band, and this would give rise to the observed softening process accompanied by a steep decay of the flux density. The curvature effect scenario predicts that the terminating time of the softening process would be correlated with the duration of the process. In this paper, on the basis of the data from the UNLV GRB (University of Nevada, Las Vegas, Gamma-Ray Burst) group web-site, we found an obvious correlation between the two quantities. In addition, we found that the softening process can be divided into two classes: the early type softening ($t_{\rm s,max} \leq$ '4000' s) and the late type softening ($t_{\rm s,max} >$ '4000' s). The two types of softening show different behaviors in the duration versus terminating time plot. In the relation between the variation rates of the flux density and spectral index during the softening process, a discrepancy between the two types of softening is also observed. According to their timescales and the discrepancy between them, we propose that the two types are of different

1475-7516/08/11004+15$30.00

JCAP11(2008)004

origins: the early type is of internal shock origin and the late type is of external shock origin. The early softening is related to the steep decay just following the prompt emission, whereas for the late decay one typically conceives the transition from flat decay to late afterglow decay. We suspect that there might be a great difference in Lorentz factor between the two classes, which is responsible for the observed discrepancy.

Keywords: gamma ray bursts, gamma ray burst experiments

Contents

1. Introduction

A newly discovered phenomenon, the *spectral softening* of gamma-ray bursts (GRBs) observed by the Swift instruments in their early x-ray afterglows [1]–[5], has not been predicted by any of the existing GRB models. Credit for this discovery goes to the Swift instruments, which can monitor x-ray emission of GRBs at quite early time after the trigger events. Soon after this discovery, the authors of [6] performed a systematic analysis of a selected sample of Swift bursts and found that ∼75% of the bursts (33 out of 44) show an obvious spectral softening process. Besides their papers, the UNLV (University of Nevada, Las Vegas) GRB group also presented temporal and spectral data for Swift bursts on their web-site[4]; these continue to accumulate as the number of Swift bursts keeps increasing. Their data show, besides the steep decay phase, that the softening can be observed in later phases as well (see our analysis below).

Most softening processes are detected in the steep decay phase in the early x-ray afterglows of GRBs. Since the steep decay phase promptly follows, and is smoothly connected to, the prompt emission phase, it is regarded as the prompt emission tail [7]–[10]. It is generally believed that this phenomenon is due to the high latitude emission of fireballs, in which the so-called curvature effect must play a role [6, 9], [11]–[18]. However, the steep decay tails are expected from the curvature effect but the softening process is not, which puzzled astronomers.

The curvature effect arises from the emission from the surface of a relativistically expanding fireball, where the delay of time, the shifting of the intrinsic spectrum due

[4] http://swift.physics.unlv.edu/

to high latitude emission areas, as well as other relevant factors of expanding fireballs must be taken into account (for detailed explanation and analysis, see [17], [19]–[21]). Due to the great amount of energy release, relativistically expanding fireballs would be produced at a very early epoch of GRBs [22, 23]. The curvature effect is thus expected in the prompt gamma-ray emission phase. Investigations on the profile of the light curves of pulses, the spectral lags, the power-law relation between the pulse width and the energy, the evolution of the hardness ratio and the evolution of the peak energy in the prompt emission phase have been performed by various groups in the last decade [19]–[21], [24]–[34]. It was shown that the effect can also play an important role in the early afterglow period [11, 12, 17, 35].

There have only been a few attempts at interpreting the softening phenomenon, which indicate that the phenomenon is beyond the expectation of current or underlying models. The few attempts at interpretation include: cooling of the internal shock region might be responsible for strong softening [6]; at least in some bursts, the softening might be accounted for by the central engine, which is assumed to produce a soft and decaying afterglow emission [1, 6, 36]; both the temporal behavior and the spectral softening of bursts might be a consequence of the cannonball model of GRBs [37]; a hard-to-soft behavior lasting to the latest phases of the afterglow can be expected on the basis of the 'fireshell' model with a 'canonical GRB' light curve containing two sharply different components [38, 39]. One of the most remarkable investigations on this issue was performed by authors of [16]. They concluded that the early emission in >90% of early afterglows has a curved νf_ν spectrum and that $E_{\rm peak}$ (peak energy) likely evolves from the γ-rays through the soft x-ray bands on timescales of 10^2–10^4 s after the GRBs. Along with this is the discovery of [5]: the $E_{\rm peak}$ of GRB 060 614, which is one of the members of the sample of reference [6], decreases to as low as ∼8 keV at the beginning of the XRT observations. The same phenomenon was revealed in the literature as early as 2000 by the analysis of BeppoSAX data: the peak energy was found to evolve from the prompt to the afterglow phase of GRBs, decreasing from >700 keV to <3 keV for some bursts [40].

Motivated by the finding of reference [16], very recently, the author of [35] has shown that the curvature effect alone can produce both the softening and the decaying behavior observed in the early x-ray afterglow of the Swift bursts. It is due the shifting of the Band function spectrum [41] which gives rise to the softening along with the temporal decaying. Two factors of the curvature effect, the time delay and the variation of the Doppler effect of higher latitude emission from the fireball surface, cause the shifting of the Band function spectrum.

According to the curvature effect scenario, the start time of the softening is much smaller than the terminating time of the process, and thus it is expected that the softening duration must be correlated with its terminating time [35]. We will investigate statistically in the following whether the two quantities are correlated or not. At the same time, some other statistical properties will also be explored. We will not limit our analysis to the steep decay phase, but instead, any softening detected in the XRT light curve will be considered.

The paper is organized as follows: in section 2, we describe our sample of Swift data and the data reduction; in section 3, we discuss the statistical properties obtained from our analysis; conclusions of the present work are reported in the last section.

JCAP11(2008)004

2. Data

The data (up to 23 May 2008) employed in our analysis on the relation between the duration and terminating time of the softening process are taken from the UNLV GRB group web-site (see footnote 4), where Swift/XRT time-resolved spectra of selected bursts are available (see [6] for selection criteria for the bursts). The softening is observed in some of the bursts and we selected only those bursts which have noticeable x-ray softening, i.e., those bursts which should contain at least three data points starting from a smaller spectral index and ending at a larger one (refer to the time intervals presented in table 1 and the corresponding spectral evolution figures presented on the UNLV GRB group web-site).

The start time ($t_{\rm s,min}$) and the terminating time ($t_{\rm s,max}$), together with the corresponding values of the spectral index ($\beta_{\rm min}$ and $\beta_{\rm max}$), for the softening process of the selected bursts are listed in table 1. Here we divide the softening process into two distinct classes according to the corresponding terminating time: for class 1, $t_{\rm s,max} \leq$ '4000' s (called the early type softening); and for class 2, $t_{\rm s,max} >$ '4000' s (called the late type softening). Note that, for some bursts, there might exist both types of softening (see table 1).

An example of selecting the softening as well as the corresponding start time and terminating time is displayed in the lower panel of figure 1 (note that we employ index β instead of Γ), where the spectral evolution of GRB 070520B is shown. The light curve of this burst is displayed in the upper panel of the figure. The spectral and light curve data are taken from http://swift.physics.unlv.edu/ (spectra.txt and lc.txt files). We first selected $t_{\rm s,min}$ and $t_{\rm s,max}$ by viewing the β versus t plot (see the lower panel of figure 1 and the dash lines there), and then located them in the spectra.txt file of the burst, and then read and calculated (see the explanation below) their values as well as their uncertainties from this file. The data provided have been analyzed by the UNLV GRB group. The details of the analysis are described in [6]. The UNLV GRB group have developed a time filter for the time-resolved spectral analysis which can be automatically performed. Time intervals for analyzing the spectral index are determined by two criteria raised by them, and hence they are different from each other. For example, for GRB 070520B, the lower limit of the time interval associated with its $\beta_{\rm min} = 1.196 \pm 0.054$ is $t_1 = 125$ s and the upper limit of this interval is $t_2 = 195$ s (see figure 1 and table 1, and also the spectra.txt file). This gives rise to a time interval of 70 s. According to the data format file, the mean time of this interval is $t = (t_1 + t_2)/2 = 160$ s and its error is $\sigma_t = (t_2 - t_1)/2 = 35$ s (see table 1). However, the lower limit of the time interval associated with $\beta_{\rm max} = 1.92 \pm 0.21$ for this burst is $t_1 = 308$ s, and the upper limit of this interval is $t_2 = 391$ s. That measures the time interval as 83 s. The mean time of this interval is $t = (t_1 + t_2)/2 = 349.5$ s and its error is $\sigma_t = (t_2 - t_1)/2 = 41.5$ s (see table 1). The UNLV GRB group use different NH for different sources. They used the XSPEC spectral fitting model: a simple power law combined with the absorptions of both our Galaxy and the GRB host galaxy, $\rm wabs^{Gal} \times zwabs^{host} \times$ power law (for bursts with known redshifts) or $\rm wabs^{Gal} \times wabs^{host} \times$ power law (for bursts whose redshifts are unknown; see [6]).

JCAP11(2008)004

Table 1. The minimum and maximum values of the spectral index ($\beta_{\rm min}$ and $\beta_{\rm max}$) and the corresponding times ($t_{\rm s,min}$ and $t_{\rm s,max}$), of the softening process of the selected bursts.

Type	Burst	$t_{\rm s,min}$ (s)	$\beta_{\rm min}$	$t_{\rm s,max}$ (s)	$\beta_{\rm max}$
Early	050315	91.0 ± 7.0	1.02 ± 0.27	620 ± 230	1.58 ± 0.45
	050421	124.0 ± 9.0	-0.23 ± 0.32	247 ± 44	1.35 ± 0.36
	050502B	340 ± 270	0.972 ± 0.053	1200 ± 150	2.29 ± 0.26
	050714B	188 ± 31	4.80 ± 0.20	474 ± 73	6.06 ± 0.40
	050716	114 ± 10	-0.13 ± 0.12	396 ± 88	1.019 ± 0.084
	050717	94.0 ± 3.0	0.08 ± 0.24	247 ± 32	0.90 ± 0.20
	050724	87.9 ± 4.3	0.38 ± 0.10	318 ± 16	2.24 ± 0.31
	050726	366 ± 32	0.72 ± 0.26	689 ± 58	1.02 ± 0.26
	050730	145 ± 12	0.245 ± 0.089	729 ± 66	0.962 ± 0.062
	050814	173.1 ± 8.1	0.885 ± 0.091	358 ± 26	1.88 ± 0.25
	050904	182 ± 13	0.043 ± 0.072	533 ± 48	0.977 ± 0.093
	050922B	673 ± 17	0.93 ± 0.29	1460 ± 220	2.21 ± 0.41
	051117A	153 ± 40	$0.722 \pm 0.02\ 8$	1560 ± 170	1.268 ± 0.027
	051227	112 ± 11	0.21 ± 0.20	340 ± 140	0.91 ± 0.31
	060115	126.7 ± 4.5	0.71 ± 0.14	810 ± 290	1.60 ± 0.31
	060124	559 ± 31	0.032 ± 0.023	871 ± 49	1.591 ± 0.087
	060210	113.0 ± 9.0	0.472 ± 0.093	500 ± 120	1.503 ± 0.049
	060211A	202 ± 16	0.689 ± 0.058	351 ± 29	1.30 ± 0.20
	060218	1013 ± 13	0.424 ± 0.087	2122 ± 27	1.057 ± 0.072
	060413	132 ± 11	0.626 ± 0.099	278 ± 31	1.25 ± 0.21
	060510B	291 ± 11	0.214 ± 0.060	417 ± 16	1.32 ± 0.18
	060522	160 ± 11	0.40 ± 0.24	390 ± 190	0.98 ± 0.16
	060526	285 ± 30	0.640 ± 0.037	429 ± 44	1.89 ± 0.13
	060607A	97 ± 10	0.428 ± 0.073	149 ± 16	1.12 ± 0.11
	060607A	229 ± 24	0.560 ± 0.061	353 ± 38	1.114 ± 0.088
	060614	104.3 ± 5.5	0.070 ± 0.042	451 ± 25	2.09 ± 0.13
	060707	213 ± 49	0.72 ± 0.15	970 ± 470	0.96 ± 0.14
	060714	116.5 ± 7.5	0.361 ± 0.083	223 ± 28	2.13 ± 0.17
	060729	132.09 ± 0.50	0.94 ± 0.20	286.8 ± 7.5	4.90 ± 0.47
	060814	83.3 ± 4.8	0.241 ± 0.074	377 ± 36	1.51 ± 0.12
	060904A	76.2 ± 3.0	0.036 ± 0.079	226 ± 14	2.19 ± 0.21
	061007	106 ± 18	0.847 ± 0.032	252 ± 57	0.967 ± 0.029
	061110A	80.4 ± 3.0	1.57 ± 0.14	210 ± 15	3.23 ± 0.21
	061121	71.7 ± 2.0	-0.455 ± 0.062	155.8 ± 5.3	1.68 ± 0.31
	061222A	108.8 ± 2.3	0.80 ± 0.20	177.8 ± 9.6	2.05 ± 0.35
	070110	111 ± 10	0.79 ± 0.11	245 ± 25	1.32 ± 0.26
	070129	299 ± 46	0.250 ± 0.030	1030 ± 150	2.36 ± 0.44
	070223	121.0 ± 3.0	-0.22 ± 0.26	218 ± 22	1.17 ± 0.13
	070318	174 ± 22	0.19 ± 0.12	397 ± 89	0.924 ± 0.069
	070330	141 ± 54	0.43 ± 0.27	540 ± 230	0.76 ± 0.20
	070419B	106 ± 17	0.569 ± 0.047	333 ± 25	1.144 ± 0.076
	070518	101 ± 22	1.147 ± 0.093	226 ± 31	1.99 ± 0.15
	070520B	160 ± 35	1.196 ± 0.054	350 ± 42	1.92 ± 0.21
	070616	204 ± 65	-0.060 ± 0.028	1100 ± 100	0.72 ± 0.15
	070621	122.0 ± 2.0	1.18 ± 0.21	235 ± 39	1.56 ± 0.16
	070704	252 ± 57	0.385 ± 0.084	511 ± 26	1.07 ± 0.25
	070714B	74.0 ± 4.0	-0.11 ± 0.22	396 ± 88	1.13 ± 0.33
	070721B	265 ± 44	0.08 ± 0.16	930 ± 160	0.50 ± 0.17

JCAP11(2008)004

Table 1. (Continued.)

Type	Burst	$t_{s,min}$ (s)	β_{min}	$t_{s,max}$ (s)	β_{max}
	071031	118.0 ± 6.0	0.320 ± 0.078	252 ± 57	1.201 ± 0.035
	071112C	624 ± 140	0.43 ± 0.11	1410 ± 210	0.65 ± 0.16
	080123	124 ± 13	0.57 ± 0.10	700 ± 450	1.35 ± 0.30
	080319B	77 ± 10	0.671 ± 0.021	133 ± 18	0.761 ± 0.022
	080325	173 ± 12	0.682 ± 0.070	407 ± 62	2.188 ± 0.068
	080430	196 ± 54	0.56 ± 0.27	910 ± 270	0.91 ± 0.26
	080503	118 ± 18	0.240 ± 0.057	407 ± 62	1.55 ± 0.35
	080506	167 ± 18	0.224 ± 0.051	288 ± 35	1.03 ± 0.21
	080523	118 ± 18	1.287 ± 0.063	299 ± 45	2.15 ± 0.17
Late	050315	$40\,000 \pm 18\,000$	0.99 ± 0.10	$400\,000 \pm 130\,000$	1.31 ± 0.23
	050721	830 ± 97	0.55 ± 0.22	$20\,400 \pm 4100$	1.16 ± 0.50
	050726	4850 ± 900	0.95 ± 0.11	$19\,300 \pm 4100$	1.25 ± 0.30
	050730	4580 ± 570	0.434 ± 0.049	$22\,600 \pm 1300$	0.714 ± 0.080
	050803	9800 ± 3300	0.879 ± 0.088	$60\,000 \pm 30\,000$	1.29 ± 0.20
	050826	210 ± 95	0.63 ± 0.30	$84\,000 \pm 54\,000$	1.64 ± 0.54
	050904	$17\,800 \pm 1300$	0.730 ± 0.063	$45\,000 \pm 15\,000$	1.28 ± 0.12
	051109A	4070 ± 570	0.720 ± 0.093	$56\,800 \pm 6200$	1.11 ± 0.18
	060105	4820 ± 180	0.92 ± 0.15	$81\,000 \pm 24\,000$	1.44 ± 0.19
	060204B	530 ± 140	1.03 ± 0.26	$13\,800 \pm 4100$	1.63 ± 0.16
	060306	135 ± 38	1.00 ± 0.16	$12\,500 \pm 6500$	1.39 ± 0.14
	060313	178 ± 65	0.42 ± 0.16	7100 ± 2900	1.01 ± 0.14
	060714	980 ± 220	0.78 ± 0.19	6750 ± 650	1.19 ± 0.21
	060807	4960 ± 480	1.09 ± 0.15	$17\,400 \pm 1300$	1.39 ± 0.20
	070220	397 ± 87	0.23 ± 0.20	$12\,100 \pm 1300$	0.80 ± 0.20
	070318	990 ± 220	0.55 ± 0.11	$12\,480 \pm 890$	1.01 ± 0.27
	070419B	5970 ± 180	0.50 ± 0.15	$28\,100 \pm 1200$	0.82 ± 0.11
	070508	1600 ± 270	0.55 ± 0.12	$57\,000 \pm 23\,000$	1.31 ± 0.19
	070721B	5020 ± 770	0.43 ± 0.11	$10\,610 \pm 530$	0.68 ± 0.27
	071020	630 ± 140	0.53 ± 0.11	$17\,000 \pm 1500$	1.38 ± 0.69
	071025	174 ± 22	0.412 ± 0.049	$13\,400 \pm 2100$	1.39 ± 0.30
	080207	5260 ± 530	1.69 ± 0.23	$17\,500 \pm 1400$	2.03 ± 0.42
	080319C	650 ± 190	0.535 ± 0.079	$30\,190 \pm 970$	1.30 ± 0.31
	080328	5590 ± 200	0.57 ± 0.26	$18\,200 \pm 1200$	1.33 ± 0.20
	080413B	7000 ± 1000	0.79 ± 0.10	$18\,800 \pm 1300$	1.18 ± 0.18
	080430	6490 ± 910	0.75 ± 0.16	$26\,000 \pm 4000$	0.90 ± 0.15

3. Results

3.1. Relation between the duration and terminating time of the softening process

The duration of the softening is calculated using $\Delta t_s = t_{s,max} - t_{s,min}$. The relation between Δt_s and $t_{s,max}$ for these bursts is displayed in figure 2. We find that the data ($t_{s,max}$, Δt_s) for the selected bursts are distributed mainly within the area confined by the lines represented by $\Delta t_s = t_{s,max}$ and $\Delta t_s = t_{s,max}/2$. We observed a difference between the two types of softening: the ($t_{s,max}$, Δt_s) data for the late type softening are well within the aforementioned area, while some of the data for the early type softening dropped out the aforementioned area (especially when $t_{s,max}$ is relatively small).

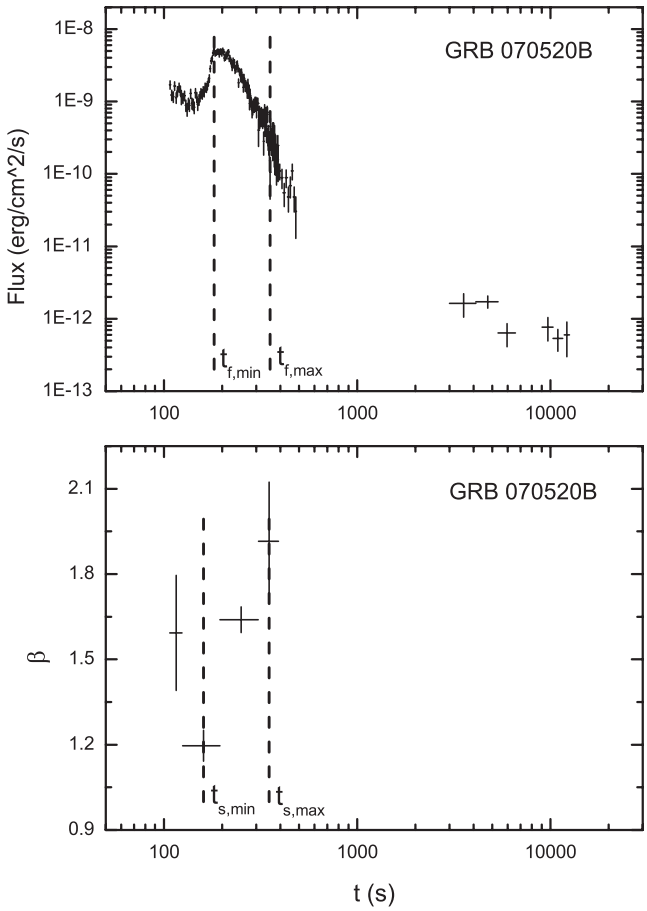

Figure 1. The spectral evolution (the lower panel) and light curve (the upper panel) of GRB 070520B. The data are taken from http://swift.physics.unlv.edu/ (see the spectra.txt and the lc.txt files of GRB 070520B). The dashed lines in the lower panel denote the time positions of $t_{\rm s,min}$ and $t_{\rm s,max}$, and those in the upper panel represent those of $t_{f,\rm min}$ and $t_{f,\rm max}$.

We performed a Spearman correlation analysis and obtained: for the early type softening, $\log \Delta t_{\rm s} = (1.172 \pm 0.051) \log t_{\rm s,max} - (0.69 \pm 0.14)$, and the fitting parameters are $R = 0.951$ (the correlation coefficient), $N = 57$ (the number of data points), and $P = 8.64 \times 10^{-30}$ (the chance probability); for the late type softening, $\log \Delta t_{\rm s} = (1.026 \pm 0.040) \log t_{\rm s,max} - (0.19 \pm 0.18)$, with $R = 0.982$, $N = 26$, and $P = 7.51 \times 10^{-19}$. This is in good agreement with the prediction made from the curvature effect [35]. In addition, the results show that the correlation between the two quantities for the late type softening follows well the trend of the identical curve, while in some extent it departs from the identical curve for the early type softening (see also figure 2). The cause of this difference is currently not known.

3.2. Two types of softening distinguished in other aspects

In addition to the duration and terminating time of the softening process, we also measured the variations of the spectral index and the flux density during this period.

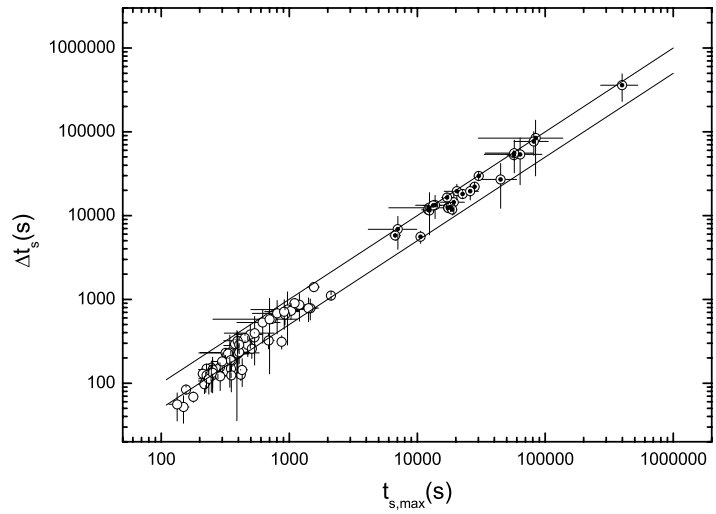

Figure 2. Relation between the duration $\Delta t_{\rm s}$ and the terminating time $t_{\rm s,max}$ of the softening process observed in the x-ray afterglows of the selected bursts. The upper and lower solid lines are drawn as $\Delta t_{\rm s} = t_{\rm s,max}$ and $\Delta t_{\rm s} = t_{\rm s,max}/2$, respectively. Open circles and open circles with dots represent the early type softening and the late type softening, respectively.

The period of the softening is confined by the lower limit (t_1) of the interval that measures $\beta_{\rm min}$ and the upper limit (t_2) of the interval that measures $\beta_{\rm max}$. For example, for GRB 070520B, the lower limit of the time interval associated with its $\beta_{\rm min} = 1.196 \pm 0.054$ is $t_1 = 125$ s, and the upper limit of the time interval associated with its $\beta_{\rm max} = 1.92 \pm 0.21$ is $t_2 = 391$ s (see section 4), and thus the softening period of this burst is the time interval from 125 to 391 s. Within this period, we search for the minimum and maximum of the flux f_ν from the lc.txt file of GRB 070520B. The two extreme values of the flux are denoted by $f_{\nu,\rm min}$ and $f_{\nu,\rm max}$ respectively, and the corresponding times are denoted by $t_{f,\rm min}$ and $t_{f,\rm max}$ respectively. The values of $t_{f,\rm min}$ and $t_{f,\rm max}$ and their uncertainties are estimated in the same way as was adopted in measuring $t_{\rm s,min}$ and $t_{\rm s,max}$ and their uncertainties (see section 4). For GRB 070520B, we found $f_{\nu,\rm max} = (52.7 \pm 3.9) \times 10^{-10}$ erg cm^{-2} s^{-1}, $f_{\nu,\rm min} = (10.5 \pm 6.1) \times 10^{-11}$ erg cm^{-2} s^{-1}, $t_{f,\rm max} = 181.6 \pm 1.0$ s, and $t_{f,\rm min} = 353.6 \pm 1.0$ s (see table 2). One might observe that for this burst $t_{f,\rm max}$ is different from $t_{\rm s,min}$ and $t_{f,\rm min}$ is different from $t_{\rm s,max}$. Two facts cause this difference. The first is that time intervals for measuring the flux are generally smaller than those for measuring the spectral index (see figure 1, where the number of data points of the flux within the softening period is much larger than that of the spectral index). The second is that in the softening process some bursts undergo a rise phase and then a decay phase in the light curve, and close to the lower limit of the softening we measure the peak of the flux instead of the flux at the very beginning of the softening process (see also figure 1). (Note that we identified a softening process according to the spectral index but not the flux.)

In table 2, we listed the maximum and minimum values of the flux density detected during the softening process. We calculated the variation rates of the two quantities using $\Delta\beta/\Delta t_{\rm s} = (\beta_{\rm max} - \beta_{\rm min})/\Delta t_{\rm s}$ and $\Delta \log f_\nu/\Delta t_f = (\log f_{\nu,\rm max} - \log f_{\nu,\rm min})/\Delta t_f$, where $\Delta t_f = t_{f,\rm min} - t_{f,\rm max}$ is the time interval between $f_{\nu,\rm max}$ and $f_{\nu,\rm min}$, which can be different from $\Delta t_{\rm s}$ (see table 2).

JCAP11(2008)004

Table 2. The maximum and minimum values of the flux density ($f_{\nu,\max}$ and $f_{\nu,\min}$) and the corresponding times ($t_{f,\max}$ and $t_{f,\min}$), detected during the softening process.

Type	Burst	$t_{f,\max}$ (s)	$f_{\nu,\max}$ [a]	$t_{f,\min}$ (s)	$f_{\nu,\min}$ [a]
Early	050315	88.0 ± 1.5	$(8.6 \pm 1.4) \times 10^{-10}$	620 ± 77	$(12.8 \pm 2.3) \times 10^{-12}$
	050421	130.4 ± 1.0	$(17.1 \pm 3.4) \times 10^{-10}$	285.0 ± 4.7	$(9.6 \pm 4.5) \times 10^{-11}$
	050502B	743.2 ± 1.0	$(66.6 \pm 4.6) \times 10^{-10}$	1277 ± 26	$(29.5 \pm 9.8) \times 10^{-12}$
	050714B	162.4 ± 1.0	$(19.2 \pm 2.6) \times 10^{-8}$	273.2 ± 3.5	$(2.2 \pm 1.5) \times 10^{-9}$
	050716	109.0 ± 1.0	$(25.1 \pm 3.1) \times 10^{-10}$	457.0 ± 1.0	$(9.0 \pm 4.5) \times 10^{-11}$
	050717	96.0 ± 1.0	$(32.2 \pm 3.9) \times 10^{-10}$	202.0 ± 1.0	$(15.1 \pm 9.2) \times 10^{-11}$
	050724	79.94 ± 0.25	$(18.6 \pm 2.1) \times 10^{-9}$	312.0 ± 1.1	$(7.6 \pm 2.4) \times 10^{-10}$
	050726	382.3 ± 6.9	$(17.3 \pm 2.9) \times 10^{-11}$	617.8 ± 8.6	$(5.9 \pm 1.4) \times 10^{-11}$
	050730	139.6 ± 1.0	$(20.5 \pm 2.4) \times 10^{-10}$	603.6 ± 1.0	$(22.4 \pm 6.7) \times 10^{-11}$
	050814	167.09 ± 0.30	$(24.6 \pm 4.1) \times 10^{-10}$	363.7 ± 2.9	$(17.0 \pm 3.2) \times 10^{-11}$
	050904	178.0 ± 1.0	$(34.6 \pm 3.4) \times 10^{-10}$	566.0 ± 1.0	$(14.8 \pm 5.6) \times 10^{-11}$
	050922B	755.6 ± 1.6	$(5.7 \pm 1.0) \times 10^{-9}$	1426 ± 12	$(19.1 \pm 8.6) \times 10^{-12}$
	051117A	134.0 ± 1.0	$(87.3 \pm 5.7) \times 10^{-10}$	1257.7 ± 1.1	$(41.5 \pm 9.3) \times 10^{-11}$
	051227	114.2 ± 1.0	$(11.7 \pm 2.1) \times 10^{-10}$	460 ± 10	$(10.5 \pm 7.4) \times 10^{-12}$
	060115	124.45 ± 0.25	$(32.9 \pm 6.2) \times 10^{-10}$	741 ± 32	$(19.4 \pm 4.6) \times 10^{-12}$
	060124	572.14 ± 0.25	$(84.1 \pm 5.8) \times 10^{-9}$	849.50 ± 0.70	$(10.8 \pm 2.1) \times 10^{-10}$
	060210	106.8 ± 1.0	$(64.9 \pm 5.6) \times 10^{-10}$	302.8 ± 1.0	$(13.6 \pm 6.8) \times 10^{-11}$
	060211A	187.0 ± 1.0	$(47.1 \pm 3.6) \times 10^{-10}$	379.0 ± 1.0	$(10.9 \pm 5.5) \times 10^{-11}$
	060218	1258.04 ± 0.25	$(18.0 \pm 4.0) \times 10^{-9}$	1975.54 ± 0.25	$(39.3 \pm 9.3) \times 10^{-10}$
	060413	122.0 ± 1.0	$(12.5 \pm 1.0) \times 10^{-9}$	302.8 ± 1.8	$(7.7 \pm 2.2) \times 10^{-10}$
	060510B	305.53 ± 0.25	$(12.1 \pm 1.5) \times 10^{-9}$	442.59 ± 0.77	$(29.8 \pm 9.4) \times 10^{-11}$
	060522	158.2 ± 1.0	$(5.3 \pm 1.2) \times 10^{-10}$	461.4 ± 7.2	$(10.3 \pm 7.7) \times 10^{-12}$
	060526	255.78 ± 0.61	$(14.8 \pm 1.2) \times 10^{-9}$	463.4 ± 1.0	$(14.6 \pm 5.5) \times 10^{-11}$
	060607A	99.8 ± 1.0	$(84.9 \pm 6.4) \times 10^{-10}$	153.8 ± 1.0	$(50.5 \pm 9.7) \times 10^{-11}$
	060607A	267.8 ± 1.0	$(38.9 \pm 2.8) \times 10^{-10}$	387.8 ± 1.0	$(14.0 \pm 4.9) \times 10^{-11}$
	060614	106.03 ± 0.25	$(75.2 \pm 5.6) \times 10^{-9}$	465.2 ± 3.6	$(43.6 \pm 5.2) \times 10^{-11}$
	060707	188.3 ± 3.5	$(17.0 \pm 3.3) \times 10^{-11}$	1301 ± 28	$(4.1 \pm 1.8) \times 10^{-12}$
	060714	139.6 ± 1.0	$(72.7 \pm 4.5) \times 10^{-10}$	223.6 ± 1.0	$(13.9 \pm 7.3) \times 10^{-11}$
	060729	132.34 ± 0.25	$(11.8 \pm 1.1) \times 10^{-8}$	276.48 ± 0.51	$(21.9 \pm 6.9) \times 10^{-10}$
	060814	79.84 ± 0.25	$(45.3 \pm 4.6) \times 10^{-9}$	365.8 ± 1.5	$(9.9 \pm 1.6) \times 10^{-10}$
	060904A	74.44 ± 0.25	$(37.1 \pm 3.8) \times 10^{-9}$	214.86 ± 0.68	$(4.1 \pm 1.4) \times 10^{-10}$
	061007	91.4 ± 1.0	$(39.5 \pm 1.7) \times 10^{-9}$	306.96 ± 0.58	$(37.2 \pm 4.8) \times 10^{-10}$
	061110A	86.64 ± 0.25	$(9.9 \pm 1.3) \times 10^{-9}$	198.37 ± 0.30	$(15.3 \pm 5.1) \times 10^{-10}$
	061121	74.91 ± 0.25	$(19.2 \pm 1.1) \times 10^{-8}$	154.29 ± 0.75	$(12.5 \pm 2.2) \times 10^{-10}$
	061222A	109.82 ± 0.25	$(13.0 \pm 1.9) \times 10^{-9}$	175.7 ± 1.1	$(19.7 \pm 3.6) \times 10^{-10}$
	070110	102.0 ± 1.0	$(13.8 \pm 1.7) \times 10^{-10}$	249.1 ± 4.2	$(9.9 \pm 2.1) \times 10^{-11}$
	070129	365.0 ± 1.0	$(26.5 \pm 1.5) \times 10^{-9}$	1054 ± 10	$(2.4 \pm 1.1) \times 10^{-11}$
	070223	118.9 ± 1.0	$(40.3 \pm 4.9) \times 10^{-10}$	231.0 ± 1.0	$(6.6 \pm 1.9) \times 10^{-10}$
	070318	274.8 ± 1.0	$(17.3 \pm 2.2) \times 10^{-10}$	482.8 ± 1.0	$(12.3 \pm 5.5) \times 10^{-11}$
	070330	221.9 ± 2.9	$(29.5 \pm 6.1) \times 10^{-11}$	616 ± 16	$(13.5 \pm 5.1) \times 10^{-12}$
	070419B	104.0 ± 1.0	$(15.8 \pm 1.0) \times 10^{-9}$	352.0 ± 1.0	$(16.1 \pm 2.1) \times 10^{-10}$

JCAP11(2008)004

Table 2. (Continued.)

Type	Burst	$t_{f,\max}$ (s)	$f_{\nu,\max}$ [a]	$t_{f,\min}$ (s)	$f_{\nu,\min}$ [a]
	070518	104.0 ± 1.0	$(12.9 \pm 1.6) \times 10^{-10}$	256.0 ± 1.0	$(4.0 \pm 2.9) \times 10^{-11}$
	070520B	181.6 ± 1.0	$(52.7 \pm 3.9) \times 10^{-10}$	353.6 ± 1.0	$(10.5 \pm 6.1) \times 10^{-11}$
	070616	486.0 ± 1.0	$(20.0 \pm 1.2) \times 10^{-9}$	1174.8 ± 5.4	$(15.7 \pm 4.0) \times 10^{-11}$
	070621	124.8 ± 1.0	$(61.9 \pm 5.1) \times 10^{-10}$	272.8 ± 1.0	$(11.7 \pm 8.3) \times 10^{-11}$
	070704	315.2 ± 1.0	$(106.5 \pm 7.9) \times 10^{-10}$	535.2 ± 1.0	$(2.7 \pm 1.6) \times 10^{-10}$
	070714B	73.5 ± 1.0	$(24.3 \pm 3.2) \times 10^{-10}$	466.1 ± 6.0	$(1.5 \pm 1.0) \times 10^{-11}$
	070721B	312.0 ± 1.0	$(25.8 \pm 2.7) \times 10^{-10}$	935.6 ± 5.4	$(3.1 \pm 1.9) \times 10^{-11}$
	071031	121.4 ± 1.0	$(58.2 \pm 4.1) \times 10^{-10}$	305.4 ± 1.0	$(5.5 \pm 1.0) \times 10^{-10}$
	071112C	569.1 ± 2.4	$(27.9 \pm 6.8) \times 10^{-11}$	1413.8 ± 7.2	$(2.2 \pm 1.1) \times 10^{-11}$
	080123	122.0 ± 1.0	$(17.7 \pm 2.1) \times 10^{-10}$	921 ± 77	$(6.9 \pm 4.9) \times 10^{-13}$
	080319B	68.2 ± 1.0	$(135.9 \pm 3.4) \times 10^{-9}$	150.09 ± 0.91	$(45.7 \pm 2.0) \times 10^{-9}$
	080325	222.2 ± 1.0	$(108.3 \pm 7.4) \times 10^{-10}$	460.2 ± 1.0	$(5.0 \pm 1.6) \times 10^{-10}$
	080430	172.3 ± 6.0	$(21.1 \pm 5.3) \times 10^{-11}$	603 ± 15	$(2.4 \pm 1.1) \times 10^{-11}$
	080503	105.2 ± 1.0	$(48.4 \pm 3.9) \times 10^{-10}$	409.3 ± 5.0	$(3.1 \pm 1.4) \times 10^{-11}$
	080506	156.4 ± 1.0	$(57.4 \pm 4.4) \times 10^{-10}$	320.4 ± 1.0	$(5.3 \pm 3.8) \times 10^{-11}$
	080523	104.8 ± 1.0	$(19.9 \pm 2.0) \times 10^{-10}$	306.8 ± 1.0	$(10.2 \pm 4.6) \times 10^{-11}$
Late	050315	23810 ± 270	$(9.7 \pm 1.1) \times 10^{-12}$	$432\,400 \pm 9400$	$(40.8 \pm 7.4) \times 10^{-14}$
	050721	777.0 ± 5.0	$(14.1 \pm 3.4) \times 10^{-11}$	$23\,530 \pm 190$	$(8.8 \pm 6.2) \times 10^{-13}$
	050726	4001 ± 53	$(27.3 \pm 6.6) \times 10^{-12}$	$23\,010 \pm 380$	$(10.7 \pm 2.9) \times 10^{-13}$
	050730	4370.1 ± 3.7	$(5.2 \pm 1.0) \times 10^{-10}$	$23\,912 \pm 28$	$(7.2 \pm 2.9) \times 10^{-12}$
	050803	$10\,502 \pm 53$	$(5.7 \pm 4.0) \times 10^{-11}$	$83\,100 \pm 5500$	$(9.7 \pm 1.4) \times 10^{-13}$
	050826	169.7 ± 5.0	$(20.8 \pm 5.1) \times 10^{-11}$	$111\,000 \pm 12\,000$	$(10.4 \pm 6.8) \times 10^{-14}$
	050904	$18\,582.8 \pm 8.9$	$(8.6 \pm 1.8) \times 10^{-11}$	$47\,020 \pm 120$	$(4.9 \pm 3.4) \times 10^{-13}$
	051109A	4185 ± 32	$(61.0 \pm 8.3) \times 10^{-12}$	$57\,940 \pm 670$	$(27.2 \pm 5.3) \times 10^{-13}$
	060105	5571.2 ± 3.4	$(24.4 \pm 5.7) \times 10^{-11}$	$87\,600 \pm 300$	$(12.6 \pm 4.8) \times 10^{-13}$
	060204B	411 ± 17	$(11.6 \pm 1.9) \times 10^{-11}$	$16\,720 \pm 110$	$(2.1 \pm 1.1) \times 10^{-12}$
	060306	102.4 ± 1.7	$(10.3 \pm 1.5) \times 10^{-10}$	$16\,970 \pm 220$	$(40.3 \pm 9.5) \times 10^{-13}$
	060313	149.4 ± 2.4	$(27.2 \pm 6.1) \times 10^{-11}$	4500 ± 17	$(3.0 \pm 2.1) \times 10^{-12}$
	060714	880 ± 10	$(8.4 \pm 1.8) \times 10^{-11}$	6860 ± 28	$(3.7 \pm 2.1) \times 10^{-12}$
	060807	4743 ± 53	$(36.6 \pm 4.9) \times 10^{-12}$	$17\,850 \pm 250$	$(62.4 \pm 9.5) \times 10^{-13}$
	070220	542.5 ± 3.5	$(41.0 \pm 8.0) \times 10^{-11}$	$12\,786 \pm 53$	$(4.1 \pm 2.5) \times 10^{-12}$
	070318	789.1 ± 4.1	$(15.8 \pm 3.8) \times 10^{-11}$	7584 ± 39	$(2.8 \pm 2.0) \times 10^{-12}$
	070419B	5807.5 ± 3.8	$(17.3 \pm 4.3) \times 10^{-11}$	$29\,245 \pm 19$	$(6.1 \pm 4.6) \times 10^{-12}$
	070508	1583.3 ± 2.4	$(8.0 \pm 2.1) \times 10^{-10}$	$53\,632 \pm 269$	$(11.7 \pm 8.3) \times 10^{-13}$
	070721B	4438 ± 15	$(40.4 \pm 9.5) \times 10^{-12}$	$10\,501 \pm 38$	$(5.1 \pm 2.4) \times 10^{-12}$
	071020	566.6 ± 2.9	$(31.4 \pm 6.8) \times 10^{-11}$	$17\,000 \pm 1500$	$(11.4 \pm 3.6) \times 10^{-13}$
	071025	159.0 ± 1.0	$(100.8 \pm 7.5) \times 10^{-10}$	$10\,866 \pm 39$	$(2.3 \pm 1.3) \times 10^{-12}$
	080207	4751 ± 19	$(17.3 \pm 4.1) \times 10^{-11}$	$18\,230 \pm 100$	$(9.8 \pm 4.6) \times 10^{-12}$
	080319C	505.1 ± 7.7	$(44.9 \pm 6.0) \times 10^{-11}$	$30\,511 \pm 35$	$(1.8 \pm 1.3) \times 10^{-12}$
	080328	5517 ± 14	$(15.0 \pm 3.4) \times 10^{-11}$	$18\,298 \pm 43$	$(4.9 \pm 3.0) \times 10^{-12}$
	080413B	8541 ± 53	$(3.5 \pm 1.4) \times 10^{-11}$	$12\,367 \pm 53$	$(2.1 \pm 1.5) \times 10^{-12}$
	080430	5965 ± 35	$(14.2 \pm 3.5) \times 10^{-12}$	$29\,943 \pm 57$	$(2.2 \pm 1.1) \times 10^{-12}$

[a] In units of erg cm^{-2} s^{-1}.

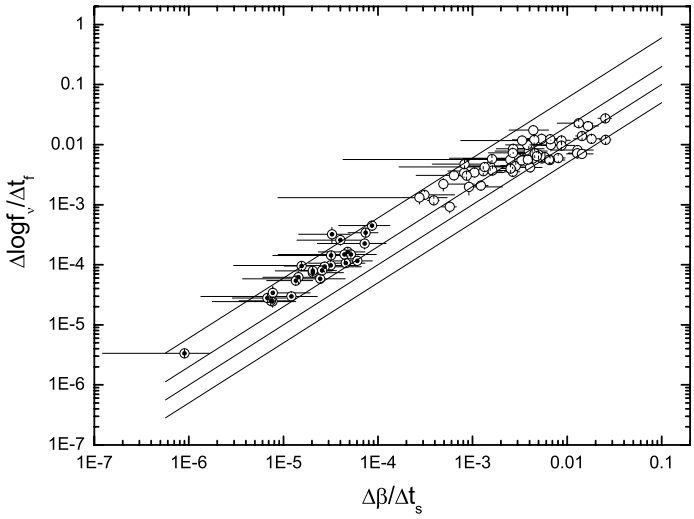

Figure 3. Relation between the variation rates of the flux density and spectral index, $\Delta \log f_\nu/\Delta t_f$ and $\Delta\beta/\Delta t_\mathrm{s}$, during the softening process observed in the x-ray afterglows of the selected bursts. Solid lines from top to the bottom represent the $\Delta \log f_\nu/\Delta t_f = k\Delta\beta/\Delta t_\mathrm{s}$ lines with $k = 6$, 2, 1, and 0.5, respectively. The open circles represent the early type softening while the open circles with dots represent the late type softening.

In figure 3, we present the relation between the two variation rates. It shows that the two types of softening do have distinct behaviors in the variation rate. Data for the late type softening are distributed within the $\Delta \log f_\nu/\Delta t_f = 2\Delta\beta/\Delta t_\mathrm{s}$ and $\Delta \log f_\nu/\Delta t_f = 6\Delta\beta/\Delta t_\mathrm{s}$ curves, which follow well the trend of the identical curve. For the early type softening, the data are scattered in a wider area confined by the $\Delta \log f_\nu/\Delta t_f = 0.5\Delta\beta/\Delta t_\mathrm{s}$ and $\Delta \log f_\nu/\Delta t_f = 6\Delta\beta/\Delta t_\mathrm{s}$ curves. The trend of the early type is obviously deviated from that of the identical curve.

A Spearman correlation analysis for the two variation rates was also performed. For the early type softening we got $\log \Delta \log f_\nu/\Delta t_f = (0.556 \pm 0.045) \log \Delta\beta/\Delta t_\mathrm{s} - (0.85 \pm 0.11)$, with $R = 0.857$, $N = 57$, and $P = 1.84 \times 10^{-17}$, and for the late type softening we obtained $\log \Delta \log f_\nu/\Delta t_f = (0.987 \pm 0.071) \log \Delta\beta/\Delta t_\mathrm{s} + (0.51 \pm 0.33)$, with $R = 0.943$, $N = 26$, and $P = 5.49 \times 10^{-13}$. The correlation must be owing to the fact that the softening scope (represented by $\Delta\beta$) and the decaying scale (described by $\Delta \log f_\nu$) vary mildly for different sources, but the time intervals of the process differ significantly. The two types of softening occupy distinct areas in the plot due to the large difference in softening duration between them. But why the trends of the relation for the two types are so different remains unclear.

4. Discussion and conclusions

In the present work, we studied the relation between the duration and terminating time of the softening process observed in the x-ray afterglows of the Swift bursts. We found that these two quantities are obviously correlated, as expected from the curvature effect. The analysis reveals that the softening can be divided into two classes merely on the basis of

the corresponding terminating time: the early type softening ($t_{\rm s,max} \leq$ '4000' s) and the late type softening ($t_{\rm s,max} >$ '4000' s). The two types of softening show different behaviors in their duration and the terminating time plot. We also investigated the relation between the variation rates of the flux density and the spectral index during the softening process. In this respect, more obvious discrepancy is observed between the two types of softening.

As revealed in [35], the duration of the softening can be affected by three parameters: the Lorentz factor, the radius, and the intrinsic radiative peak energy concerned. As shown in [35] figure 6, for the same Lorentz factor Γ and radius R_c, a smaller intrinsic peak energy $E_{0,\rm p}$ can lead to a smaller duration of the process, while the corresponding terminating time will be unchanged. It would give rise to the departure observed in figure 2. Why does this occur in the early type softening but not in the late type softening? We suspect that probably the early type softening is of internal shock origin while the late type softening is of external shock origin. In the former case the Lorentz factor is large and thus the curvature effect is sensitive to the fireball parameters, while in the latter case the Lorentz factor is small and hence the curvature effect is less sensitive to the fireball parameters. Is it due to the selection effect? This is unlikely, because if the earlier softening tends to have a relatively small duration due to the overlapping of its start time with other components of emission, then it will affect both variation rates of the flux density and spectral index in the same way and then the possible influence will be canceled. But figure 3 clearly shows that the early softening does have a different behavior relative to the rest.

The fact that the GRBs with lowest $t_{\rm s,max}$ tend to deviate from the $\Delta t_{\rm s} \sim t_{\rm s,max}$ law may be partially due to the fact that $\Delta t_{\rm s}$ is defined as the difference of the linear quantities $t_{\rm s,max}$ and $t_{\rm s,min}$ and we take the logarithm of $\Delta t_{\rm s}$ and correlate it with the logarithm of $t_{\rm s,max}$. Is it better to use the ratio between $t_{\rm s,max}$ and $t_{\rm s,min}$ rather than $\Delta t_{\rm s}$? The ratio, when passing to logarithms, becomes the difference between $\log t_{\rm s,max}$ and $\log t_{\rm s,min}$. Is it a more suitable quantity to correlate with $\log t_{\rm s,max}$? We studied this issue by replacing $\Delta t_{\rm s}$ with $t_{\rm s,max}/t_{\rm s,min}$ in figure 2. We found a weak correlation between $\log(t_{\rm s,max}/t_{\rm s,min})$ and $\log t_{\rm s,max}$ (the plot is omitted). The data are quite scattered in the $\log(t_{\rm s,max}/t_{\rm s,min})$ versus $\log t_{\rm s,max}$ plane. The analysis does not provide any information on the causes of the mentioned deviation. This must be due to the fact that $\log(t_{\rm s,max} - t_{\rm s,min})$ is closer to $\log t_{\rm s,max}$ than $\log t_{\rm s,max} - \log t_{\rm s,min}$ is, as long as the discrepancy between $t_{\rm s,max}$ and $t_{\rm s,min}$ is large enough (say, when $t_{\rm s,max}$ is one order of magnitude larger than $t_{\rm s,min}$).

The strongest factor in favor of our suggestion of two types of origin might be that the two types of softening occur at very different timescales (the former appears much earlier and the latter emerges very late). In addition, we found that the early type softening is observed in the steep decay phase which is believed to be due to the high latitude emission of the prompt phase [6, 9], [11]–[18] and the late type softening is found in the normal afterglow phase which was believed to be due to the external shocks [42]–[44].

It should be pointed out that the softening process is divided into two classes empirically. If the two kinds of softening are associated with internal and external shock mechanisms, it might be more natural to divide them according to the start time of the process. By examining the data in tables 1 and 2, we roughly redivided the softening process into two classes according to $t_{\rm s,min}$ being less or larger than 500 s. Shown in figure 4 are the relations between the duration and the terminating time of the softening process for the newly defined early and late types. As expected, they do not dramatically affect the result. The two types are distributed in two distinguishable domains in the

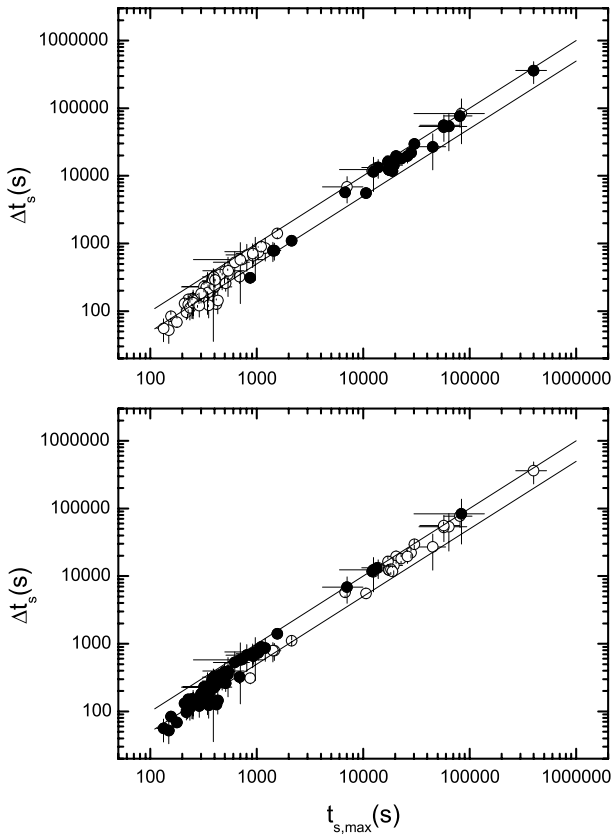

Figure 4. Relation between $\Delta t_{\rm s}$ and $t_{\rm s,max}$ for the newly defined two types of the softening process. Filled circles in the upper panel and open circles in the lower panel represent the process with $t_{\rm s,min} > 500$ s (the newly defined late type softening process). Filled circles in the lower panel and open circles in the upper panel stand for the process with $t_{\rm s,min} \leq 500$ s (the newly defined early type softening process). The two solid lines are the same as they are in figure 2.

$\Delta t_{\rm s}$ versus $t_{\rm s,max}$ plane. However, a slight overlapping between the two distributions is observed. We do not know whether this overlapping is due to the overlapping of physical parameters or merely the statistical fluctuation. One might notice that few of the new early type occupy the late type domain near the identical curve and few of the late type are located in the early type domain near the $\Delta t_{\rm s} = t_{\rm s,max}/2$ curve. Both seem to be a result of the extension of the two types. We therefore insist that this possibility cannot be ruled out with the current data. However, for an empirical analysis, we prefer the former division, i.e. dividing them according to $t_{\rm s,max}$, since no overlapping is observed in this division scenario.

Studied in figure 3 is the relation between the variation rates of the flux density and spectral index during the softening process. How would it be if we simply studied the relation between $\Delta \log f_\nu$ and $\Delta\beta$? Shown in figure 5 is the result. One finds that the two types seem to have different distributions of $\Delta \log f_\nu$ and $\Delta\beta$. The late type softening tends to have smaller $\Delta\beta$ and slightly larger $\Delta \log f_\nu$. However, the overlapping is so heavy that we cannot tell the type of a softening merely according to its location in the

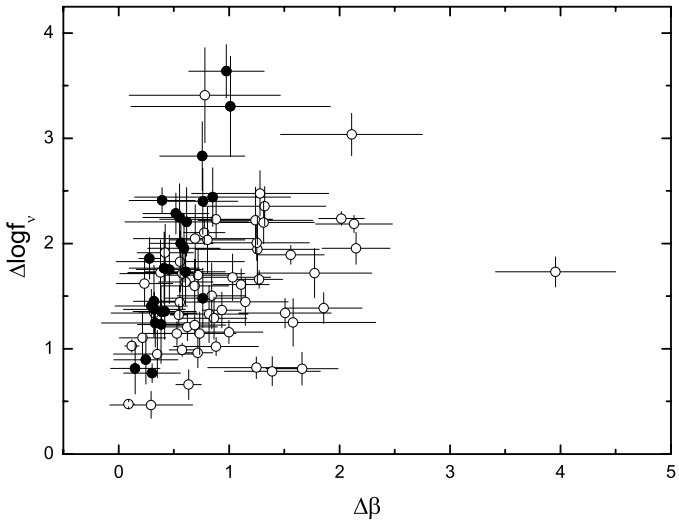

Figure 5. Relation between the variations of the flux density and the spectral index, $\Delta \log f_\nu$ and $\Delta\beta$, during the softening process observed in the x-ray afterglows of the selected bursts. Filled circles stand for the late type of softening and open circles for the early type.

$\Delta \log f_\nu$ versus $\Delta\beta$ plane. This difference, if confirmed statistically later, might become a hint in searching for the physical difference between the two softening processes.

Acknowledgments

Our special thanks are given to the anonymous referee for his or her comments and suggestions which have improved the paper greatly. This work was supported in part by the National Natural Scientific Foundation of China (10573005, 10633010, 10747001) and the 973 project (No. 2007CB815405). We also thank for financial support the Guangzhou Education Bureau and Guangzhou Science and Technology Bureau.

References

[1] Campana S *et al*, 2006 *Nature* **442** 1008 [SPIRES]
[2] Ghisellini G *et al*, 2006 *Mon. Not. R. Astron. Soc.* **372** 1699
[3] Gehrels N *et al*, 2006 *Nature* **444** 1044 [SPIRES]
[4] Zhang B *et al*, 2007 *Astrophys. J.* **655** L25 [SPIRES]
[5] Mangano V *et al*, 2007 *Astron. Astrophys.* **470** 105 [SPIRES]
[6] Zhang B B, Liang E W and Zhang B, 2007 *Astrophys. J.* **666** 1002 [SPIRES]
[7] Tagliaferri G *et al*, 2005 *Nature* **436** 985 [SPIRES]
[8] Barthelmy S D *et al*, 2005 *Astrophys. J.* **635** L133 [SPIRES]
[9] Liang E W *et al*, 2006 *Astrophys. J.* **646** 351 [SPIRES]
[10] Sakamoto T *et al*, 2007 *Astrophys. J.* **669** 1115 [SPIRES]
[11] Kumar P and Panaitescu A, 2000 *Astrophys. J.* **541** L51 [SPIRES]
[12] Dermer C D, 2004 *Astrophys. J.* **614** 284 [SPIRES]
[13] Dyks J *et al*, 2005 arXiv:astro-ph/0511699
[14] Panaitescu A *et al*, 2006 *Mon. Not. R. Astron. Soc.* **366** 1357
[15] Zhang B *et al*, 2006 *Astrophys. J.* **642** 354 [SPIRES]
[16] Butler N R and Kocevski D, 2007 *Astrophys. J.* **663** 407 [SPIRES]
[17] Qin Y-P, 2008 *Astrophys. J.* **683** 900 [SPIRES]
[18] Starling R L C *et al*, 2008 *Mon. Not. R. Astron. Soc.* **384** 504

[19] Qin Y-P, 2002 *Astron. Astrophys.* **396** 705 [SPIRES]
[20] Qin Y-P *et al*, 2004 *Astrophys. J.* **617** 439 [SPIRES]
[21] Qin Y-P *et al*, 2006 *Phys. Rev.* D **74** 063005 [SPIRES]
[22] Goodman J, 1986 *Astrophys. J.* **308** L47 [SPIRES]
[23] Paczynski B, 1986 *Astrophys. J.* **308** L43 [SPIRES]
[24] Fenimore E E *et al*, 1996 *Astrophys. J.* **473** 998 [SPIRES]
[25] Sari R and Piran T, 1997 *Astrophys. J.* **485** 270 [SPIRES]
[26] Ryde F and Petrosian V, 2002 *Astrophys. J.* **578** 290 [SPIRES]
[27] Kocevski D, Ryde F and Liang E-W, 2003 *Astrophys. J.* **596** 389 [SPIRES]
[28] Qin Y-P and Lu R-J, 2005 *Mon. Not. R. Astron. Soc.* **362** 1085
[29] Shen R-F *et al*, 2005 *Mon. Not. R. Astron. Soc.* **362** 59
[30] Lu R-J, Qin Y-P, Zhang Z-B and Yi T-F, 2006 *Mon. Not. R. Astron. Soc.* **367** 275
[31] Lu R-J, Peng Z-Y and Dong W, 2007 *Astrophys. J.* **663** 1110 [SPIRES]
[32] Peng Z-Y *et al*, 2006 *Mon. Not. R. Astron. Soc.* **368** 1351
[33] Qin Y-P *et al*, 2005 *Astrophys. J.* **632** 1008 [SPIRES]
[34] Jia L-W, 2008 *Chin. J. Astron. Astrophys.* **4** 451
[35] Qin Y-P, 2008 *Astrophys. J.* at press [arXiv:0806.3339v1]
[36] Fan Y Z *et al*, 2006 *J. Cosmol. Astropart. Phys.* JCAP09(2006)013 [SPIRES]
[37] Dado S, Dar A and Rujula A D, 2008 *Astrophys. J.* **681** 1408 [SPIRES]
[38] Ruffini R *et al*, 2006 *Astrophys. J.* **645** L109 [SPIRES]
[39] Bianco C L *et al*, 2008 *AIP Conf. Proc.* **966** 12 [SPIRES]
[40] Frontera F *et al*, 2000 *Astrophys. Suppl. Ser.* **127** 59
[41] Band D *et al*, 1993 *Astrophys. J.* **413** 281 [SPIRES]
[42] Meszaros P and Rees M J, 1997 *Astrophys. J.* **476** 232 [SPIRES]
[43] Sari R, Piran T and Narayan R, 1998 *Astrophys. J.* **497** L17 [SPIRES]
[44] Chevalier R A and Li Z-Y, 2000 *Astrophys. J.* **536** 195 [SPIRES]

JCAP11(2008)004